A Method of Deriving an Equivalent Permeability Spectrum of Ferrous Materials Considering All Effects in Electrical Machines for 2-D Magneto-Dynamic Simulations

Hujun Peng and Kay Hameyer, *Senior Member, IEEE*

***Abstract*—In this article, a method is developed to calculate an equivalent permeability spectrum of ferrous materials in the context of electrical machines. Compared with the complex permeability in the literature, the calculated equivalent permeability considers all practical effects in electrical machines besides eddy current influences in the electrical steel. The equivalent permeability is calculated using the phase inductance of electrical machines. However, due to parasitic capacitance's influence in electrical machines, the phase inductance spectrum cannot be directly measured. In order to solve the problem, a grey box method is applied to model electrical machines in a wide frequency range. Then, all electrical components related to the parasitic capacitors are removed from the grey box model, and the remaining electrical circuit is used to determine the phase inductance spectrum without the parasitic capacitors' influence. Finally, the phase inductance spectrum calculated from the grey box model is compared with the FEM-simulated inductance spectrum to search for the equivalent permeability in a wide frequency range. Since the phase inductance spectrum contains all practical effects in electrical machines, the calculated equivalent permeability also includes these effects. The searched equivalent permeability can be used for 2-D magneto-dynamic simulations, whose results are required for parametrizing the white box models.**

***Index Terms*—Complex permeability, electrical machine, grey box model, high-frequency modeling, high-frequency permeability, permanent magnet synchronous motor, White box model.**

I. Introduction

SEMICONDUCTOR modules with wide bandgaps, such as SiC and GaN, are increasingly applied in automotive applications owing to their low switching losses, high switching frequency, and high-temperature endurance. However, a high voltage slew rate, resulting from the fast switching of these semiconductor power modules, leads to a large voltage overshoot at the machine's terminals [1]. These high-voltage oscillations happen due to the interaction of inverters, cables, and electrical machines [2]. Furthermore, a high voltage slew rate leads to uneven electrical potential distribution along the stator windings, which increases the potential difference between neighboring conductors [3]. It leads to an increased risk of partial discharges. These phenomena usually occur in voids inside the insulation system, damaging the insulation material and leading to premature failure of the electric machine [4]. In low-voltage electrical machines with an effective voltage below 700 V, partial discharges must be avoided over the entire lifetime according to IEC 60034-18-41 [5]. If the voltage distribution along the winding is known, the insulation system can be designed appropriately [6]. For this purpose, high-frequency white box models of electrical machines are needed to calculate the voltage distribution along stator winding. The white box model considers inductive and capacitive coupling in electrical machines up to several megahertz. For inductive coupling, frequency-dependent self-impedance and mutual impedance among conductors must be considered [6]. In implementing the white box models, each conductor in electrical machines is modeled and connected according to the winding schema to create an electrical network. The equivalent electrical circuit of each conductor in the white box model is parameterized using finite-element-analysis (FEA) results [7], [8]. Before running the FEA simulations, one of the most crucial challenges is determining the frequency-dependent equivalent permeability [9]. The equivalent permeability is used in 2-D magneto-dynamic simulations. 2-D simulations are used because the computational load for applying 3-D simulations to capture the skin effect at frequencies above megahertz is prohibited since the skin depth is in the range of several micrometers. Therefore, 2-D simulations with the equivalent permeability are adopted in the literature. The state-of-the-art method of calculating such an equivalent permeability is presented in the following equation and it considers the eddy current effects in the laminated steel sheets [10], [11]:

$$\mu_{\text{lamination}} = \mu_{\text{steel}} \cdot \frac{\tanh\left((1+j)\cdot b/\delta\right)}{(1+j)\cdot b/\delta} \tag{1}$$

Manuscript received 10 September 2023; revised 21 November 2023, 21 January 2024, and 12 March 2024; accepted 9 April 2024. Date of publication 29 May 2024; date of current version 11 October 2024. This work was supported by Toyota Motor Corporation. *(Corresponding author: Hujun peng.)*

The authors are with the Institute of Electrical Machines (IEM), RWTH Aachen University, 52062 Aachen, Germany (e-mail: hujun.peng@iem.rwth-aachen.de).

Color versions of one or more figures in this article are available at https://doi.org/10.1109/TIE.2024.3390744.
Digital Object Identifier 10.1109/TIE.2024.3390744

whereby b is the half of silicon steel sheet thickness, δ is the skin depth dependent on frequency, and μ_{steel} is a permeability value. The permeability in (1) is a complex number, varying with changing frequency. Differences among works lie in choosing the factor μ_{steel} for applying the equivalent complex permeability in (1). For example, in [12], the differential permeability at the averaged flux density of the entire electrical machine is used, while in [13], the absolute permeability at the average flux density is used.

There are some limitations in using the complex permeability in (1). Many important effects except the eddy current effects in the laminated steel are not considered, including magnetic aftereffect, hysteresis, domain wall resonance, production influences during motor assembly, and other phenomena in the silicon steel sheet [14]. More importantly, the factor μ_{steel} in (1) is calculated based on the average value of flux density in electrical machines, which does not consider the local distribution of the flux density. Therefore, the simulated inductance using the complex permeability in (1) does not necessarily reflect the electrical machine's measured inductance. Therefore, the equivalent permeability considering all effects in the context of electrical machines is much more complex than that given in (1). After the literature study, no publications have proposed a method of calculating an equivalent permeability considering all effects in the context of electrical machines. This equivalent permeability should be consistent with the inductance measured at motor terminals. This work aims to fill this gap, and the following contributions will be contained.

1) A thought of determining the equivalent permeability based on phase inductance spectra of electrical machines is proposed. The difficulty in directly measuring the phase inductance of electrical machines is explained. A method of estimating the phase inductance spectrum with influences from the parasitic capacitors removed is emphasized.
2) A high-frequency grey box model is developed for modeling a permanent magnet synchronous machine (PMSM) with interior magnets in rotors. Then, the components related to the parasitic capacitors are removed from the grey box model, and the remaining electrical circuit helps determine the phase inductance spectrum with the parasitic capacitors' influence removed.
3) FEM simulation with an eddy current solver is used to search the equivalent permeability in the context of electrical machines by comparing the FEM simulated phase inductance to the derived phase inductance values.

The organization of the work is as follows: In Section II, the phase inductance spectrum of electrical machines is introduced, and parasitic capacitors' influence on the measuring results is emphasized. Section III introduces impedance measurement setups for high-frequency modeling of a PMSM. Then, a grey box model is developed based on the impedance measurement. In Section IV, the grey box model is validated in the frequency domain. After that, in Section V, the equivalent permeability considering all effects in electrical machines is searched based on comparing the FEM simulated inductance and the derived inductance values from the grey box model. Finally, Section VII gives conclusions and outlooks.

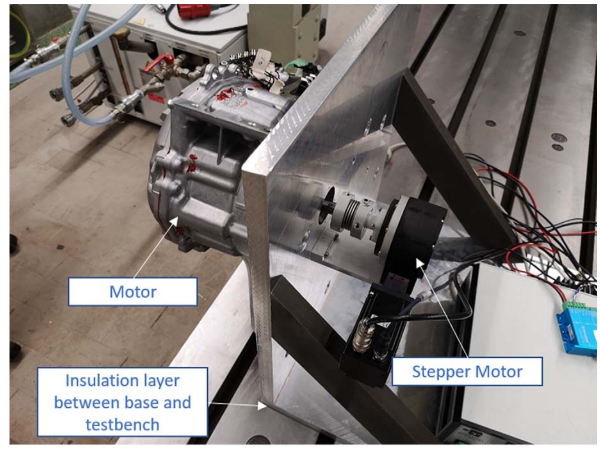

Fig. 1. Impedance measurement setup of the PMSM.

II. Difficulty in Directly Measuring Phase Inductance Spectra of Electrical Machines

This section will introduce the phase impedance measurement of an entire PMSM with hairpin windings. The difficulty in directly measuring winding inductance up to megahertz is emphasized.

Fig. 1 presents the PMSM on the test bench. An insulation layer is inserted between the electrical machine and the test bench to reduce the electromagnetic interference from the test bench, which has a large metallic surface and works like an antenna in the high-frequency domain. The PMSM has a pole pair number of four, and the slot number is 48. Each slot has eight conductors, and each phase's conductors are connected in serials. Therefore, each phase has 128 conductors connected in serials. Eight conductors in serials form a coil, and then, each phase consists of 16 coils connected in serials. In addition, a stepper motor is coupled to the PMSM to change its rotor position.

The impedance spectrum between terminal U and the neutral point (NP) is displayed in Fig. 2(a). The impedance amplitude is normalized using the impedance amplitude at 100 Hz. The phase inductance can be calculated using the impedance amplitude and phase information, as shown in (2), whereby $|Z|$ and ϕ represent impedance amplitude and phase, respectively. Fig. 2(b) presents the calculated phase inductance. It is observed that the calculated phase inductance decreases from 100 Hz to about 12 kHz, which corresponds to the skin effect phenomena. However, the calculated phase inductance increases after 12 kHz, which contradicts the decreasing trend of inductance under the skin effects. Its explanation is that the electrical machines' parasitic capacitors start to influence the measured impedance spectrum strongly. These capacitors lie between neighboring conductors in one slot as well as between the conductors and the stator iron

$$L_{\text{calculated}} = \frac{|Z| \cdot \sin(\phi)}{2 \cdot \pi \cdot f}. \quad (2)$$

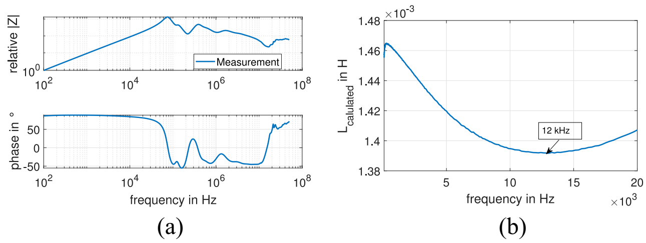

Fig. 2. Impedance measurement results: (a) Impedance spectrum between phase U and the NP of the PMSM. (b) Calculated phase U inductance based on the measured impedance spectrum.

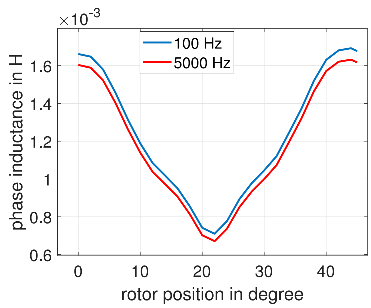

Fig. 3. Comparison of the calculated phase inductances between 100 and 5000 Hz.

The calculated phase inductance at 100 and 5000 Hz, dependent on rotor position, is compared in Fig. 3. The phase inductance shows a mechanical degree period of 45° since there are eight poles in the PMSM. Regarding the maximum phase inductance, the value of 1.632 mH at 5000 Hz is less than the inductance of 1.679 mH at 100 Hz by about 3%.

The polarization curves of the steel sheet used in the PMSM are also measured using the single sheet tester. The thickness of the steel sheet is about 0.26 mm, and the density is about 7400 kg/m^3. The apparent and differential relative permeability as functions of flux density is displayed for 100 and 5000 Hz in Fig. 4. The definitions of the apparent and differential permeability are presented in Fig. 2(c), whereby the apparent permeability corresponds to the ratio between the magnetic flux density and the field strength at the operation point, and the differential permeability is related to the slope of the tangential line at the operation point. The differential permeability is much smaller than the absolute permeability after comparing the apparent permeability in Fig. 4(a) and the differential permeability in Fig. 4(b). Most importantly, the difference in the measured permeability between 100 and 5000 Hz, either for the absolute or the differential permeability, is much more significant than the relative difference in the calculated phase inductance in Fig. 3. Therefore, the equivalent magnetic permeability required for high-frequency modeling electrical machines differs from the directly measurable permeability using the single sheet tester. One possible reason is that the equivalent permeability derived from the impedance measurement of electrical machines contains all effects in the context of electrical machines, including magnetic saturation effects due to the interior permanent

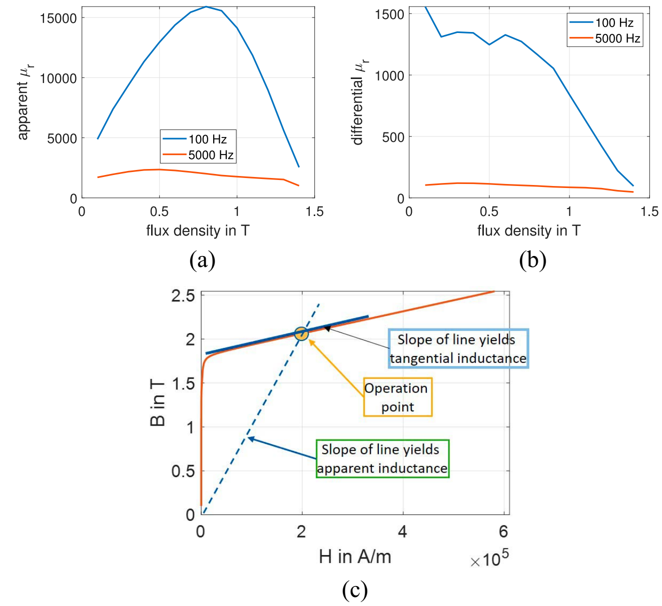

Fig. 4. Comparison of permeability of the silicon steel sheet between 100 and 5000 Hz: (a) Apparent permeability. (b) Differential permeability. (c) Explanation of the apparent and incremental differential permeability.

magnets in the rotor. However, these effects are not considered using the single sheet tester.

Summarily, the equivalent magnetic permeability used for the white box modeling is assumed to correspond to the high-frequency phase inductance measured on electrical machines' terminals. It differs from that measured using the single sheet tester. In order to calculate the equivalent permeability, the phase inductance can be used to derive the equivalent permeability of ferrous materials in the context of electrical machines. Since the phase inductance contains all effects in the electrical machines, the derived equivalent permeability also considers comprehensive influences. However, the frequency range, in which the phase inductance of electrical machines can be directly measured without influences of parasitic capacitors, is limited to several kilo-hertz. This frequency range is not enough for white box modeling of electrical machines. Therefore, a method will be developed in the next section to estimate the phase inductance up to mega-hertz with the parasitic capacitors' influence removed.

III. Grey Box Modeling of PMSM Based on Impedance Spectrum Measurement

In this section, various impedance spectra of the electrical machine are measured, whose results are used to develop and parameterize the grey box model.

The impedance analyzer "Keysight E4990A" is used to measure the impedance spectrum from 100 Hz to 10 MHz. Different motor terminal connection setups are applied to measure the impedance spectra, as shown in Table. I. The configuration setups include phase-to-NP, phase-to-phase, phase-to-housing, and phase-to-two-phases. The symbol "NP" stands for the NP,

TABLE I
MOTOR TERMINAL CONNECTION TYPES FOR MEASURING IMPEDANCE SPECTRA OF THE PMSM

Symbol	Meaning
U-GND	Impedance between phase U and housing
V-GND	Impedance between phase and housing
W-GND	Impedance between phase and housing
UVW-GND	Impedance between UVW and housing
U-NP	Impedance between phase U and NP
V-NP	Impedance between phase V and NP
W-NP	Impedance between phase W and NP
U-V	Impedance between phase U and V
V-W	Impedance between phase V and W
W-U	Impedance between phase W and U
U-VW	Impedance between phase U and VW
V-WU	Impedance between phase V and WU
W-UV	Impedance between phase W and UV

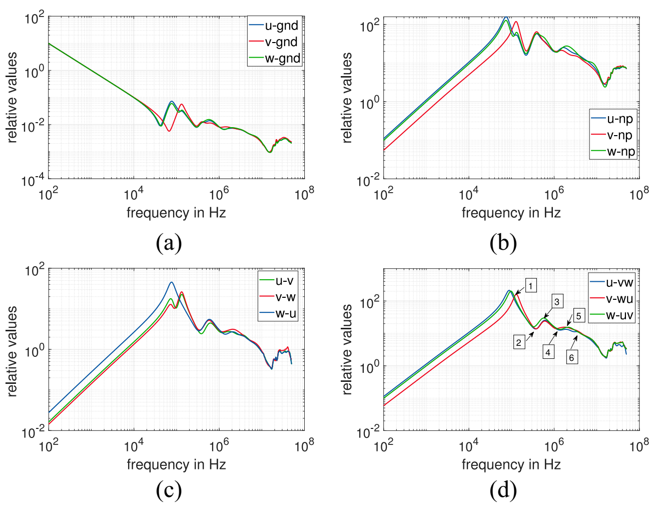

Fig. 5. Motor impedance spectra for different terminal connection types. (a) Phase-to-housing. (b) Phase-to-NP. (c) Phase-to-phase. (d) Phase-to-two-phases.

"GND" represents housing, and "UV" means the short-circuit connection between terminal U and V.

The impedance spectra for different terminal connection types are shown in Fig. 5, including the phase-to-housing impedance in Fig. 5(a), the phase-to-NP impedance in Fig. 5(b), the phase-to-phase impedance in Fig. 5(c), and the phase-to-two-phases impedance in Fig. 5(d). At low frequencies, the impedance amplitude in Fig. 5(b)–5(d) shows a difference among the three phases due to the asymmetry between the d and q axes in the PMSM with internal magnets in its rotor. However, the impedance spectra of different phases overlap to a large degree at high frequencies because the asymmetry decreases with higher frequencies. Therefore, in developing a high-frequency grey box model of the PMSM, the deviation at low frequencies and the similarity at high frequencies among phases must be considered in the parameterization process. No works in the literature have modeled PMSM with interior permanent magnets in rotors for grey box modeling. One goal of the article is to model the six primary resonance points below 5 MHz in the impedance spectra, which are marked in Fig. 5(d).

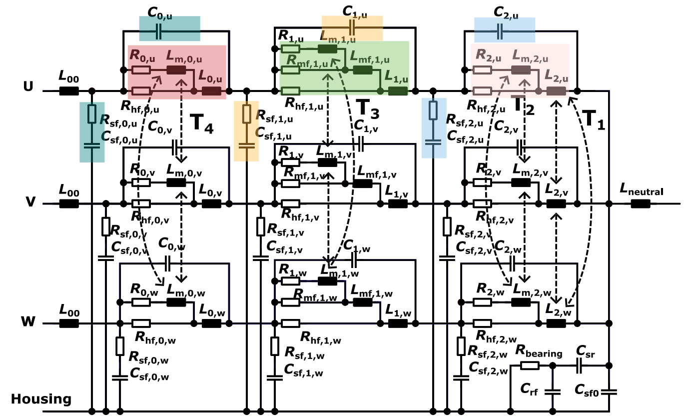

Fig. 6. Grey box model with four mutual inductances $T_1 - T_4$ among phases, symbolized with dashed lines.

The following parts will explain a grey box method to model all marked primary resonance points.

Fig. 6 presents the electrical circuit of the grey box model of the PMSM to be developed. Resonant points occur due to the interaction between capacitances and inductances. Since six main resonant points are observed in the impedance spectra in Fig. 5, an electrical circuit with three branches is proposed, as shown in Fig. 6. Thereby, each branch corresponds to a pair of resonance points.

The branches are numbered "0", "1", and "2". The first index in each electrical component in Fig. 6 indicates its corresponding branch number. Branch 2 represents the part of one phase winding close to the NP. Branch 0 represents the outermost part of one phase winding near motor terminals. Branch 1 describes the middle part of one phase winding between branch 2 and 0.

In the following explanation, phase U is used as an example to explain how the proposed grey box model generates six main resonance points in the impedance spectra. In branch 2 of phase U, the inductive and capacitive elements are marked in different colors. The inductive part is modeled using an "RL"-network, which considers the skin effect. The capacitive part contains two sections, one for the winding-to-housing capacity and the other for the winding-to-winding capacity. Besides the capacitors, another electrical resistor $R_{\mathrm{sf,x,x}}$ is used to represent the resistance in the insulation layer between windings and housing in the common mode path.

In the low-frequency range, all capacitors in the equivalent electrical circuit in Fig. 6 can be treated as open circuits and neglected because they do not influence impedance spectra at low frequencies. Therefore, the remaining electrical circuit without any capacitor is purely an "RL"-ladder-network. In this case, the impedance increases with frequency before the first resonant point in Fig. 5(d).

With higher frequency, the capacitances in branch 2 begin to short circuit the inductive part in branch 1. It results in the first resonance point, and the impedance amplitude falls after the first resonance point.

Above the first resonance point frequency, the inductive part in branch 2 will not be considered since it has been short-circuited. For the second resonant point, the inductive parts in branches 1 and 0 begin to compensate for the capacitive part in branch 2 since the inductive parts in branches 1 and 0 are in serials connected with the capacitive part in branch 2. As a result, the impedance amplitude increases after the second resonant point.

With frequency increased to close to the third resonant point, the capacitive part in branch 1 is becoming dominant. It begins to short-circuit the inductive part in branch 1, and the impedance amplitude decreases again, which results in the third resonance point.

The remaining resonant points at higher frequencies can be explained similarly for branch 0. It is worth mentioning that compared with branches 0 and 2, the inductive part in branch 1 contains three "RL"-layers because the resonance points are mainly located in the middle-frequency range, which is strongly influenced by branch 1.

Some other parameters are explained as follows. In Fig. 6, the parameters L_{00} and L_{neutral} describe small inductances of external supply lines, used to contact the stator windings. The impedance between the stator winding and housing in each branch is represented by the resistor $R_{\text{sf},i,j}$ and the capacitor $C_{\text{sf},i,j}$ $(i = 0, 1, 2$ and $j = u, v, w)$ connected in serials. The capacitor C_{rf} represents the capacitance between the housing and the rotor. The symbol R_{bearing} represents the bearing resistance. The C_{sr} describes the capacitance between the stator winding and rotor, smaller than the stator-to-housing capacity by an order.

Due to the differences at low frequencies and the similarities at high frequencies among phases in the impedance spectra, the component values of the same type in branch 2 should have a relatively large ratio among different phases. In contrast, the component values in branches 1 and 0 for different phases must have a relatively small ratio among them.

Different from the state-of-the-art found in the literature, mutual inductances are considered in the grey box model, as shown in Fig. 6. After testing different numbers of mutual inductances, the grey box model with four mutual inductances performs best in the impedance fitting. The corresponding mutual inductances are symbolized by T_1–T_4. Three coupling factors are required besides three self-inductances for modeling each three-phase mutual inductance. For example, coupling coefficients $k_{\text{uv},1}$, $k_{\text{vw},1}$, and $k_{\text{uw},1}$ are introduced to calculate the mutual inductances T_1 in branch 2, as shown in (3), (4), (5). Other mutual inductances are determined following the same principle

$$M_{\text{uv},1} = k_{\text{uv},1} \cdot \sqrt{L_{2,\text{u}} \cdot L_{2,\text{v}}} \tag{3}$$

$$M_{\text{vw},1} = k_{\text{vw},1} \cdot \sqrt{L_{2,\text{v}} \cdot L_{2,\text{w}}} \tag{4}$$

$$M_{\text{uw},1} = k_{\text{uw},1} \cdot \sqrt{L_{2,\text{w}} \cdot L_{2,\text{u}}}. \tag{5}$$

The grey box model in Fig. 6 has 88 parameters. The differential evolution algorithm in [15] is applied to fit the model parameters, with the difference between the modeled and the measured impedance spectra as the cost function. The cost function will be defined in (9) in the next section. A group of parameters will be searched to minimize the cost function, and the impedance modeling results after parameter fitting will be shown in the next section.

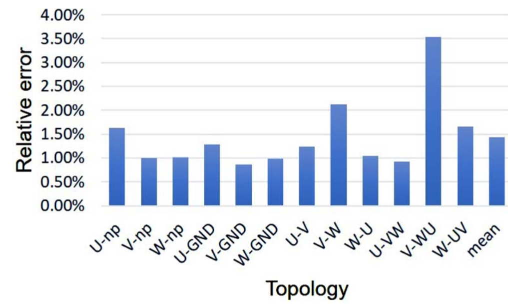

Fig. 7. Relative deviations Δ_{avg} for different motor terminal connection topologies using the grey box modeling.

IV. Validation of the Grey Box Model in the Frequency Domain

The modeled impedance spectra are compared with the measured impedance spectra for different terminal connection topologies, including phase-to-housing, phase-to-NP, phase-to-phase, and phase-to-two-phases impedance spectra. The impedance spectra of the grey box model are calculated through the embedded function within Simulink. An index $\Delta(f_i)$ is introduced to represent the modeled impedance's relative deviation from the measured values at frequency f_i, as shown in (6). Then, the index $\Delta(f_i)$ is summed over a frequency range in (7). The n is the number of frequencies at which the impedance is considered in defining the cost function used in the optimization algorithm. After that, an average deviation Δ_{avg} is calculated using (8) for each measurement topology. The parameter $\overline{\Delta}_{\text{avg}}$, as defined in (9), represents the mean value of Δ_{avg} over various measurement topologies, whereby the N represents the number of impedance measurement topologies to be considered. The optimization algorithm uses the $\overline{\Delta}_{\text{avg}}$ as the cost function

$$\Delta(f_i) = \left| \frac{|Z_{\text{model}}(f_i)| - |Z_{\text{meas}}(f_i)|}{|Z_{\text{meas}}(f_i)|} \right| \tag{6}$$

$$\Delta_{\text{sum}} = \sum_{i=1}^{\text{n}} \Delta(f_i) \tag{7}$$

$$\Delta_{\text{avg}} = \frac{\Delta_{\text{sum}}}{n} \tag{8}$$

$$\overline{\Delta}_{\text{avg}} = \frac{\sum_{i=1}^{N} \Delta_{\text{avg}}(i - \text{th topology})}{N}. \tag{9}$$

In Fig. 7, the relative deviations between the modeled and measured impedance spectra are presented for the frequency range from 1 kHz to 5 MHz for different motor terminal connection topologies. The mean relative deviation between the modeled and the measured impedance spectra is about 1.44%.

A grey box model without mutual inductances among phases is also tested for impedance modeling, and its impedance modeling results are displayed in Fig. 8. The fitting performance regarding the phase-to-NP impedance in Fig. 8(a), the phase-to-phase impedance in Fig. 8(c), the phase-to-two-phases

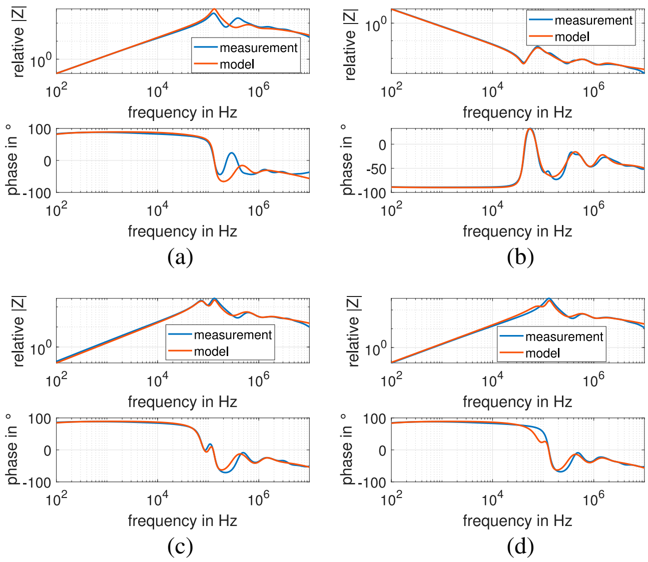

Fig. 8. Evaluation of impedance modeling without mutual inductances among phases with comparison to the measured impedance spectra. (a) V-NP. (b) U-housing. (c) U-V. (d) V-WU.

impedance in Fig. 8(d) is not satisfied in the middle-frequency range from 50 to 500 kHz. Therefore, the mutual inductances among the three phases are necessary for accurately modeling electrical machines in the high-frequency domain. One explanation lies in that the windings of three phases in electrical machines are shifted by 120 electrical degrees, and there is strong inductive coupling among them.

The impedance modeling results using the grey box model with four mutual inductances are shown in Figs. 9–12. Here, Fig. 9 stands for the phase-to-NP impedance spectra, Fig. 10 represents the phase-to-phase impedance spectra, Fig. 11 presents the phase-to-two-phases impedance spectra, and Fig. 12 describes the phase-to-housing impedance spectra. The accuracy in modeling the phase-to-NP spectra, as shown in Fig. 9, is improved, compared with that in Fig. 8(a). More significantly, the differential mode impedance spectra, as depicted in Figs. 10 and 11, overlap the measured spectra to a high degree over a wide frequency range. As a result, the accuracy of predicting the phase-to-phase voltage profiles at the motor terminals during inverter-fed operations is high. Finally, as shown in Fig. 12, the modeled phase-housing impedance spectra are extensively similar to the measured spectra. As a benefit, the accuracy in predicting the common mode and bearing voltage is increased.

In summary, the developed grey box model with mutual inductances among phases is accurate in impedance modeling. Since this article uses the phase inductance in the context of electrical machines to derive the equivalent permeability, the accuracy of the grey box model plays a crucial role.

V. Searching the Equivalent Permeability of Ferrous Materials in the Context of Electrical Machines

This section compares the phase inductance spectrum calculated from the developed grey box model to the FEM simulated

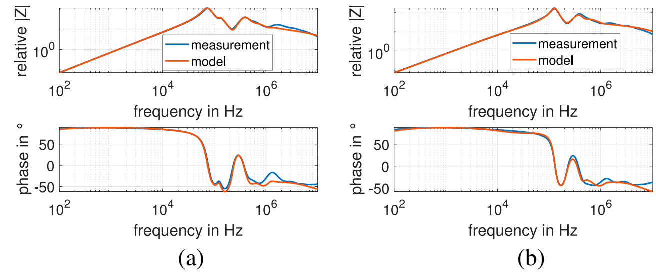

Fig. 9. Validation of the grey box model with mutual inductances in the frequency domain regarding the phase-to-NP impedance spectra: (a) U-NP and (b) V-NP.

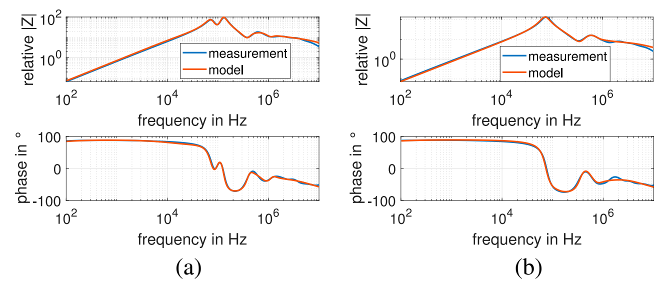

Fig. 10. Validation of the grey box model with mutual inductances in the frequency domain regarding the phase-to-phase impedance spectra: (a) U-V and (b) W-U.

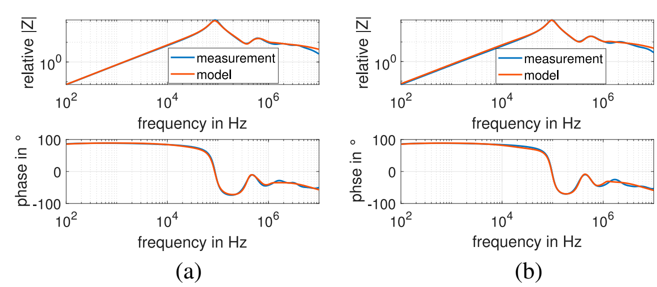

Fig. 11. Validation of the grey box model with mutual inductances in the frequency domain regarding the phase-to-two-phases impedance spectra: (a) U-VW and (b) W-UV.

inductance spectrum to search for the equivalent permeability of ferrous materials in the context of electrical machines.

In order to determine the phase inductance spectrum with the influence of parasitic capacitors, all components related to the parasitic capacitors in the developed grey box model in Fig. 6 are removed. The removed components include winding-to-winding capacitors, winding-to-housing capacitors, and winding-to-housing resistance. As a result, Fig. 13 presents the remaining electrical circuit. After that, the inductance spectrum, seen from outside terminals of the remaining model in Fig. 13, can be calculated using electrical circuit analysis tools in simulation software. The resulting inductance spectrum between phase U and the NP is presented in Fig. 17. The difficulty faced by directly measuring the phase inductance of electrical machines, mentioned in Section II, is solved. The remaining task in this section is to search for the equivalent

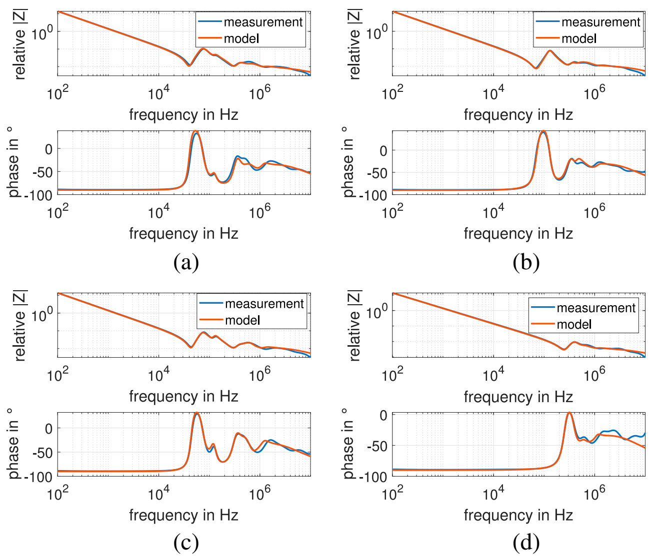

Fig. 12. Validation of the grey box model with mutual inductances in the frequency domain regarding the phase-to-housing impedance spectra: (a) U-housing. (b) V-housing. (c) W-housing. (d) UVW-housing.

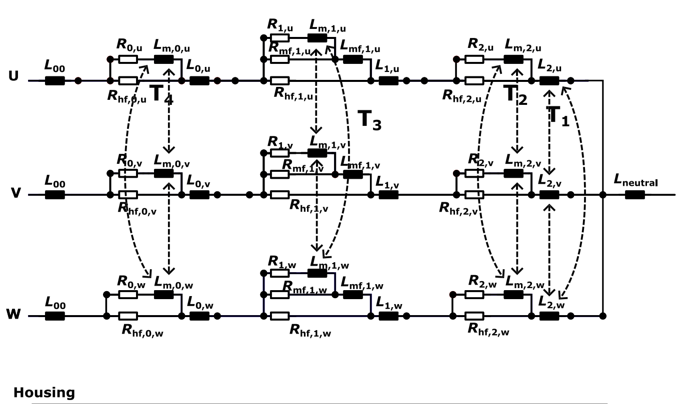

Fig. 13. Simplified grey box model with component related to parasitic capacitors removed.

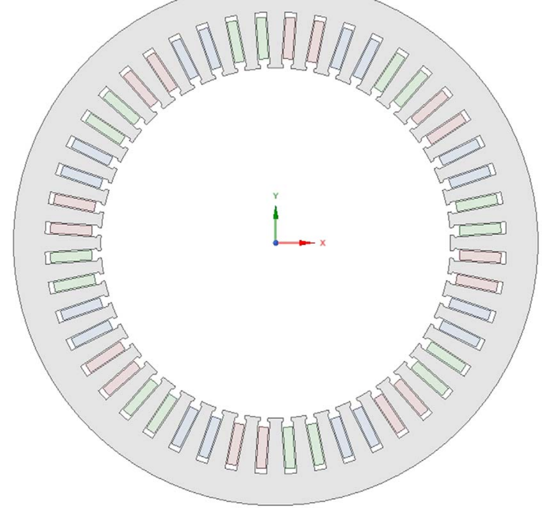

Fig. 14. Schematic 2-D-geometry of the PMSM stator.

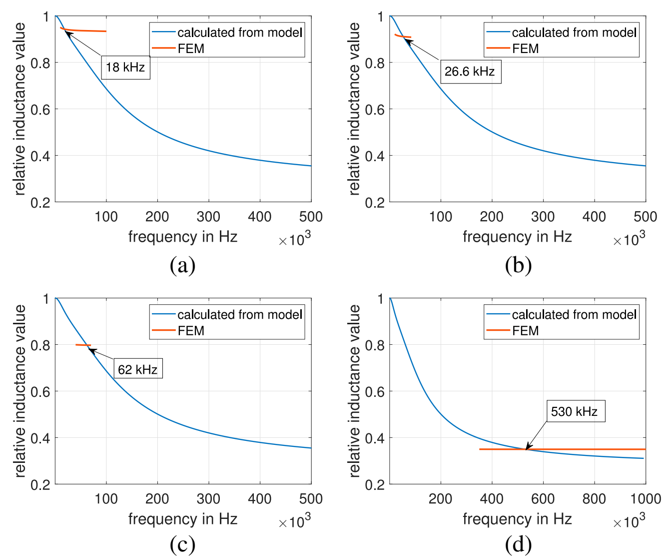

Fig. 15. Searching for the equivalent permeability up to megahertz: (a) Searching for the frequency with an equivalent permeability of $\mu_r = 1000$. (b) Frequency with $\mu_r = 700$. (c) Frequency with $\mu_r = 300$. (d) Frequency with $\mu_r = 40$.

permeability of ferrous materials using the calculated phase inductance spectrum.

Magneto-dynamic simulations are used to calculate the phase inductance spectrum. The 2-D-geometry of the PMSM is presented in Fig. 14. There are 48 slots for three phases. In each slot, there are eight hairpin conductors. Before running the FEM simulation, the most important setup for the materials is to deactivate the eddy current effect in iron materials. The reason for this setup lies in that the searched equivalent permeability already contains the eddy current effects in the laminated electrical steel. Moreover, the conductivity of the permanent magnets is set to be 0.625 MS/m.

The process of searching for the equivalent permeability is explained as follows. First, an average equivalent permeability is assumed for iron materials in electrical machines. For example, an equivalent relative permeability of 1000 is assumed. Then, the phase inductance spectrum resulting from the FEM simulation is compared with the calculated inductance spectrum based on the grey box model. It is worth mentioning that the inductance values in Fig. 15 are normalized using their peak values at 100 Hz. In Fig. 15(a), there is a cross point at 18 kHz. Therefore, the equivalent permeability of the ferrous materials at 18 kHz is found and equal to 1000. In this way, the equivalent permeability values are found for other frequencies: 700 at 26.6 kHz in Fig. 15(b), 300 at 62 kHz in Fig. 15(c), and 40 at 530 kHz in Fig. 15(d). Fig. 16 presents more equivalent permeability values in the high-frequency domain. Finally, a polynomial function is fitted based on the searched values at discrete frequencies, as shown in the following equation:

$$\mu_r = \frac{1.815 \cdot 10^7}{f} - \frac{1.803 \cdot 10^9}{f^2} + \frac{37.9}{\sqrt{f}} + 1 \qquad (10)$$

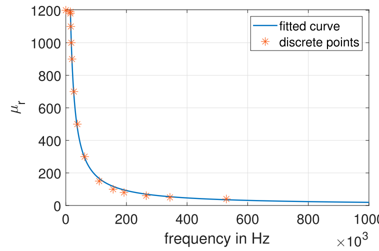

Fig. 16. Searched equivalent permeability values at various frequencies and its fitting curve.

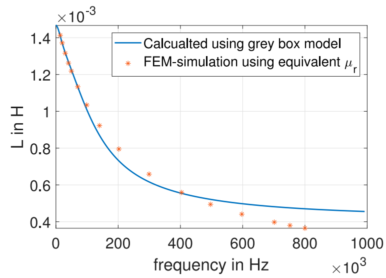

Fig. 17. Comparisons between the FEM-simulated phase inductance using the searched equivalent permeability spectrum and the inductance calculated from the grey box model.

whereby f has the unit of hertz. The equivalent permeability at 100 Hz is calculated to 1200, which is similar to the measured differential permeability in Fig. 4(b).

Finally, 2-D magneto-dynamic simulations are used again to calculate the phase inductance using the derived magnetic permeability in (10). The FEM calculated phase inductance in Fig. 17 is similar to the derived phase inductance based on the grey box model up to 600 kHz, apart from some relatively higher errors at local frequency points. The average relative error regarding the phase inductance below 600 kHz is calculated to 2.4%. The derived equivalent permeability is used for modeling white-box models in the next section.

VI. Validation of the Developed Grey Box Model and the Derived Equivalent Permeability Spectrum Based on Test Bench Measurement

In this section, the developed grey box model in Section III is firstly validated in the time domain based on test bench measurement. Then, a white-box model, created from FEM-simulation results using the derived equivalent permeability spectrum from Section V, is validated on the test bench. By validating the capability of the white-box model in predicting the voltage distribution along conductors of the PMSM, the core contribution of deriving equivalent permeability spectrum with the help of the grey box model is also verified.

A. Validation of the Grey Box Model Using Voltage Measurement on the Test Bench

Fig. 18 shows the electrical circuit of the test bench configuration. The network voltage is first rectified to generate a dc-link

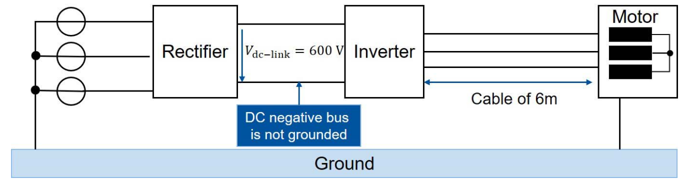

Fig. 18. Electrical circuit of the entire test bench.

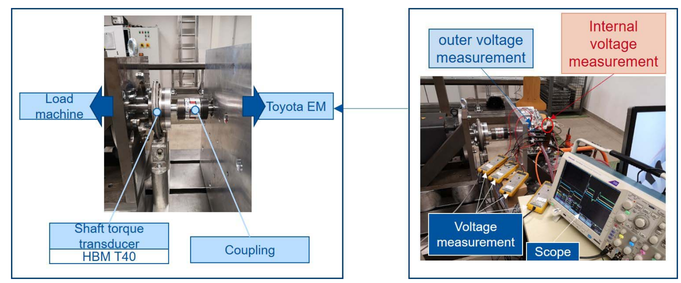

Fig. 19. Test bench configurations.

voltage of 600 V. Then, power cables connect the inverter and the electrical machine. Furthermore, the power cables' shielding and the motor housing are grounded.

The real test bench is presented in Fig. 19. The left part of Fig. 19 shows the mechanical coupling between the load machine and the PMSM under test. The coupling contains plastic materials to eliminate the influence of the load machine for validation. In the right part of Fig. 19, the voltage signals are measured at machine terminals and inside machines.

During validation of the grey box mode, the phase-to-housing signals on the inverter side are measured and used to calculate voltage signals on the machine terminals with the help of the developed grey box model. Then, the modeled voltage signals at machine terminals are compared with the corresponding measured voltage profiles. The comparison is conducted based on the raw signal data recorded in the time domain with a high sampling rate and the postprocessed voltage signal after applying the Fourier Transformation. After the postprocessing, the measured signals show much less noise than the raw signal data. The order number of the Fourier series is set to be 1000 times higher than the switching frequency, which is 2.5 kHz, to keep the computational burden affordable.

The validation process of the grey box model is conducted by comparing the common mode voltage signals in Fig. 20(a) and 20(b). The modeled and measured voltage signals between the NP and housing are compared in Fig. 20(a). The modeled and measured voltage signals between the machine terminals and housing are illustrated in Fig. 20(b). A high degree of fidelity in the voltage peak values is observed in Fig. 20. Thereby, the relative error is 1.1% between the simulated and measured voltage maximum between the NP and housing, and another error of 3.8% for the voltage between machine terminals and housing. Based on that, the accuracy of the developed grey box model is validated in the time domain.

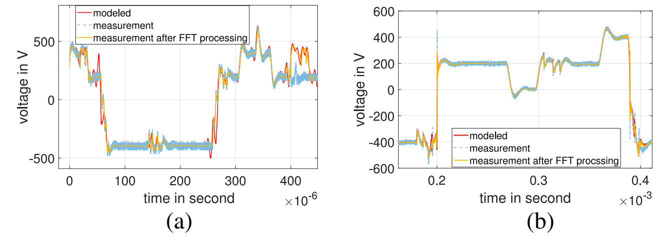

Fig. 20. Validation of the grey box model in the time domain: (a) Voltage between the NP and housing. (b) Phase-housing voltage on the machine terminals.

TABLE II
DISTRIBUTION OF THE VOLTAGE MEASURING POINTS WITHIN THE ELECTRICAL MACHINE

Symbol	Meaning
U1e / V1e	Welding point after the tenth conductor in phase U / V
U7e / V7e	Welding point after the fifty-eighth conductor in phase U / V
U8e / V8e	Welding point after the sixty-sixth conductor in phase U / V
U9e / V9e	Welding point after the seventy-fourth conductor in phase U / V

B. Validation of the Derived Equivalent Magnetic Permeability Spectrum Using Voltage Measurement on the Test Bench

The process of creating the white-box model based on FEM simulation results for the entire PMSM is not introduced since the focus of the article lies in the determination and validation of the equivalent permeability spectrum in the context of PMSM. For this purpose, some comparison examples between the measured and the simulated voltage signals along the stator windings are introduced to show that the white box model based on the developed magnetic permeability spectrum works.

It is worth mentioning that the tested PMSM's winding is modified to enable measuring voltage measurement along the stator winding, which is marked in Fig. 19. In addition, four welding points along the hairpin winding per phase are added within the PMSM, and the location of the measuring points is presented in Table II.

Fig. 21 shows the voltage measurement setups to validate the modeling of the voltage distribution along winding using the white-box model. The oscilloscope has four channels. Three of them are used to measure the voltage signals between motor terminals and housing, and the fourth channel is used to measure one voltage signal within the electrical machine. During the operation of the electrical machine, the DC-link voltage is 600 V, and the PMSM rotates at a speed of 500 min^{-1} with a q-axis current I_q of 5 A.

After comparison, the modeled conductor-to-housing voltage signals show a maximal error of 4.5% compared with the measured voltage signals for all measuring points within the electrical machines, as shown in Fig. 22. It is worth mentioning that since the validation is carried out with the help of Fourier transformation, merely the profiles during one switching period (from 0 to 0.4 ms) are used for comparison.

Fig. 23 compares the modeled and measured conductor-to-conductor voltage profiles between point U1e and point V1e.

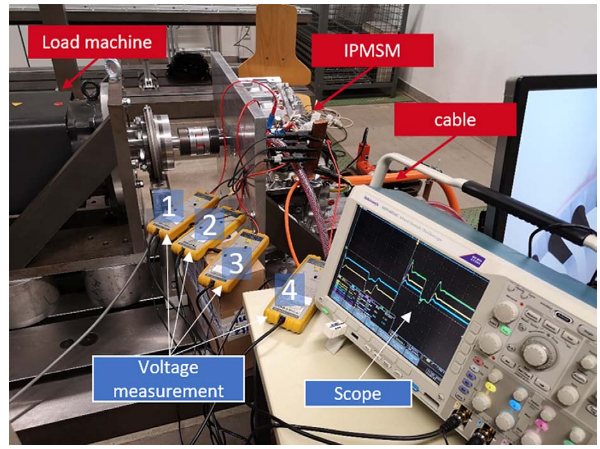

Fig. 21. oltage measurement configuration during operation of PMSM.

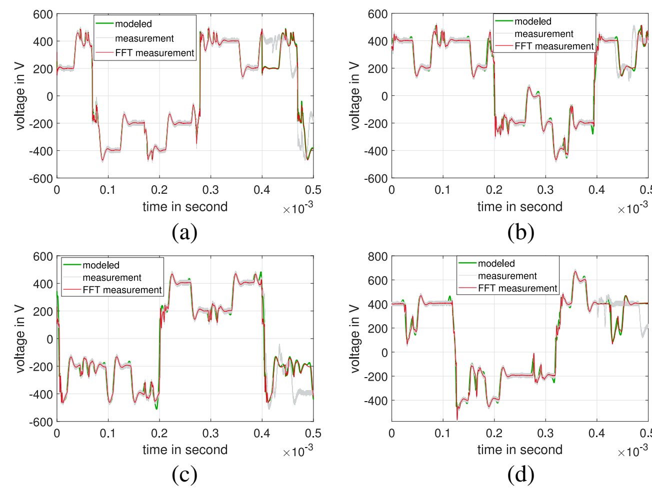

Fig. 22. Validation of the white-box model regarding conductor-housing voltages. (a) U1e to housing with an error of 2.8% between the measured and simulated voltage peak values. (b) U7e to housing with an error of 3.4%. (c) U8e to housing with an error of 4.5%. (d) U9e to housing with an error of 3.3%.

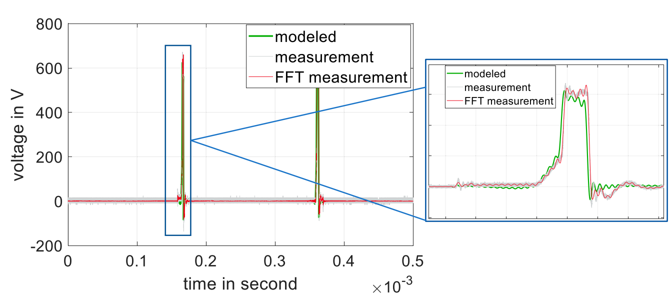

Fig. 23. Validation of the developed white-box model in the time domain regarding U1e–V1e voltage. The error is 4.5% between the simulated and measured voltage peak values.

The maximum voltage peak shows a relative error of 5.2% between measurement and white-box modeling results.

As a summary, the white-box model, created using results from FEM simulation applying the derived equivalent permeability spectrum, is validated on the test bench using an operational PMSM. Both conductor-to-housing and conductor-to-conductor voltage profiles are verified. Therefore, the derived equivalent permeability spectrum in the context of electrical machines is also verified.

VII. Conclusion

The white box modeling of electrical machines requires an equivalent permeability spectrum of ferrous materials for FEM simulations, and the equivalence means that all effects in the laminated electrical steel in the context of electrical machines are included. The complex permeability in the literature does not consider all relevant practical factors in the context of electrical machines. In order to solve the challenge, a thought of reversely deriving the equivalent permeability based on the phase inductance spectrum of electrical machines was introduced because the phase inductance contains all effects on the ferrous materials in the context of electrical machines. However, the measured phase impedance suffers enormously from parasitic capacitors' influence in electrical machines. In order to solve the problem, a grey box model was developed to model the electrical machines up to 5 MHz. After that, all components related to the parasitic capacitors were removed from the grey box model, and the remaining electrical circuit was used to calculate the phase inductance spectrum. Then, the equivalent permeability of the ferrous materials in electrical machines was searched at different frequencies by comparing the simulated phase inductance spectrum using FEM to the calculated inductance spectrum resulting from the grey box model. The core contribution of deriving permeability spectrum was indirectly validated by verifying the white box model based on the derived equivalent permeability on the test bench.

References

[1] Y. Xie, J. Zhang, F. Leonardi, A. R. Munoz, M. W. Degner, and F. Liang, "Modeling and verification of electrical stress in inverter-driven electric machine windings," *IEEE Trans. Ind. Appl.*, vol. 55, no. 6, pp. 5818–5829, Nov./Dec. 2019.

[2] G. Almandoz, S. Zarate, A. Egea, Y. Moreno, A. Urdangarin, and R. Moreno, "High frequency modeling of electric drives for electromagnetic compatibility analysis," in *Proc. Int. Conf. Elect. Mach. (ICEM),* Gothenburg, Sweden, 2020, pp. 1129–1135.

[3] F. Pauli, N. Driendl, S. Mönninghoff, and K. Hameyer, "Comparison of concentrated winding topologies considering transient voltages in the winding system of inverter-driven low-voltage machines," *Arch. Elect. Eng.*, vol. 71, no. 4, pp. 865–880, 2022.

[4] M. Kaufhold, H. Aninger, M. Berth, J. Speck, and M. Eberhardt, "Electrical stress and failure mechanism of the winding insulation in PWM-inverter-fed low-voltage induction motors," *IEEE Trans. Ind. Electron.*, vol. 47, no. 2, pp. 396–402, Apr. 2000.

[5] Rotating electrical machines—Part 18-41: Partial discharge free electrical insulation systems (type I) used in rotating electrical machines fed from voltage converters—Qualification and quality control tests, IEC Standard 60 034-18-41, Ed. I, Nov. 2014.

[6] J. Dittmann, M. England, and B. Ponick, "Design of hairpin windings considering the transient potential distribution," *e & i Elektrotechnik und Informationstechnik*, vol. 140, no. 2, pp. 271–280, 2023.

[7] J. Dittmann, M. England, and B. Ponick, "Prediction of the voltage distribution in a inverter-fed hairpin stator winding," in *Proc. 25th Int. Conf. Elect. Mach. Syst. (ICEMS)*, Piscataway, NJ, USA: IEEE Press, 2022, pp. 1–6.

[8] O. Magdun, S. Blatt, and A. Binder, "Calculation of stator winding parameters to predict the voltage distributions in inverter fed AC machines," in *Proc. 9th IEEE Int. Symp. Diagnostics Electric Mach., Power Electron. Drives (SDEMPED)*, Valencia, Spain, 2013, pp. 447–453.

[9] D. A. Hewitt, S. Sundeep, J. Wang, and A. Griffo, "High frequency modelling of electric machines using finite element analysis derived data," *IEEE Trans. Ind. Electron*., vol. 71, no. 2, pp. 1432–1442, Feb. 2024.

[10] J. Lammeraner and M. Stafl, *Eddy Current*. London, U.K.: ILIFFE Books, 1966.

[11] K. G. N. B. Abeywickrama, T. Daszczynski, Y. V. Serdyuk, and S. M. Gubanski, "Determination of complex permeability of silicon steel for use in high-frequency modeling of power transformers," *IEEE Trans. Magn.*, vol. 44, no. 4, pp. 438–444, Apr. 2008.

[12] B. Heidler, K. Brune, and M. Doppelbauer, "High-frequency model and parameter identification of electrical machines using numerical simulations," in *Proc. IEEE Int. Electric Mach. Drives Conf. (IEMDC)*, Coeur d'Alene, ID, USA, 2015, pp. 1221–1227.

[13] J. E. Ruiz-Sarrió, F. Chauvicourt, J. Gyselinck, and C. Martis, "High-frequency modelling of electrical machine windings using numerical methods," in *Proc. IEEE Int. Electric Mach. Drives Conf. (IEMDC)*, Hartford, CT, USA, 2021, pp. 1–7.

[14] C. Zhang, Y. Wang, T. Long, and X. Huang, "Voltage distribution analysis of high DV/DT fed machines using high frequency winding model," in *Proc. IEEE Transp. Electrific. Conf. Expo, Asia-Pacific (ITEC Asia-Pacific)*, Haining, China, 2022, pp. 1–6, doi: 10.1109/ITECAsia-Pacific56316.2022.9942032.

[15] Y. Zhang, H. Peng, and W. Hofmann, "Transient skin effect in highly dynamic induction motor drives: Energy-optimized design," *Elect. Eng.*, vol. 105, no. 2, pp. 1015–1024, 2023.

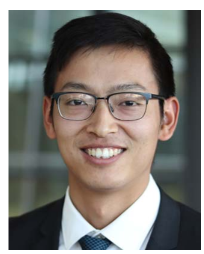

Hujun Peng received the M.Sc. degree in electrical engineering from Dresden University of Technology, Dresden, Germany, in 2017, and the Ph.D. degree in engineering from RWTH Aachen University, Aachen, Germany, in 2023.

He started working as a Research Associate with the Institute of Electrical Machines, Rheinisch-Westfälische Technische Hochschule (RWTH) Aachen University, in 2018. His research interests include high-frequency modeling of electrical machines, energy management of fuel cell hybrid vehicles, characterization of insulation systems, and analyzing parasitic effects in electrical machines.

Kay Hameyer (Senior Member, IEEE) received the M.Sc. degree in electrical engineering from the University of Hannover, Hannover, Germany, in 1986, and the Ph.D. degree in engineering from the University of Technology Berlin, Berlin, Germany, in 1992, for working on permanent magnet excited machines.

After his university studies, he worked with the Robert Bosch GmbH, Stuttgart, Germany, as a Design Engineer for permanent magnet servo motors. From 1988 to 1993, he was a Member of staff with the University of Technology Berlin. From 1996 to 2004, he was then a Full Professor in numerical field computations and electrical machines with Katholieke Universiteit Leuven (KU Leuven), Leuven, Belgium. Since 2004, he has been a Full Professor and the Director of the Institute of Electrical Machines (IEM), RWTH Aachen University, Aachen, Germany. The characterization and modeling of hard- and soft-magnetic materials is another focus of his work. He has authored/coauthored more than 350 journal publications, more than 700 international conference publications and four books. His research interest focuses on all aspects of the design, control and manufacturing of electrical machines and the associated numerical simulation. His research interests include numerical field computation and optimization, the design and control of electrical machines, in particular, permanent-magnet excited machines, induction machines.

Dr. Hameyer is a Member of the German VDE and a fellow of the Institution of Engineering and Technology, U.K.